Table of Content **Page**

*Supplemental Tables 1-3 are mentioned in the main manuscript, and Supplemental Tables 4-7 are included in the Supplemental Method section in this document.

SUPPLEMENTAL FIGURES & LEGENDS

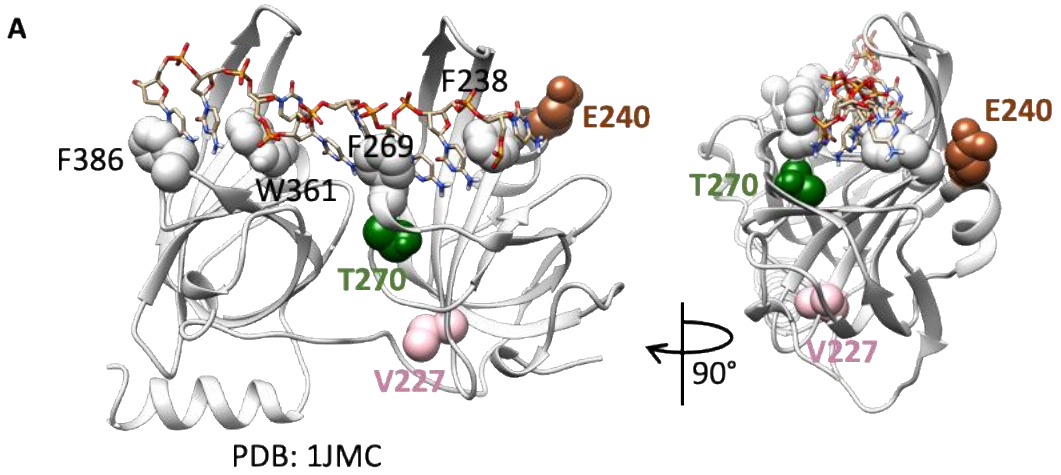

Supplemental Figure 1. Human *RPA1* variants localize to DNA binding domain A and are well conserved. A, Structure of human RPA1 highlighting affected residues V227 (pink), E240 (brown) and T270 (green) with 4 conserved aromatic residues (F238, F269, W361, F386) labeled (Protein Data Bank (PDB): 1JMC). **B**, Sequence alignments showing conservation at affected amino acid residues across 10 vertebrates. PhyloP evolutionary conservation across 100 vertebrates and PhastCons evolutionary constraint scores are shown below.

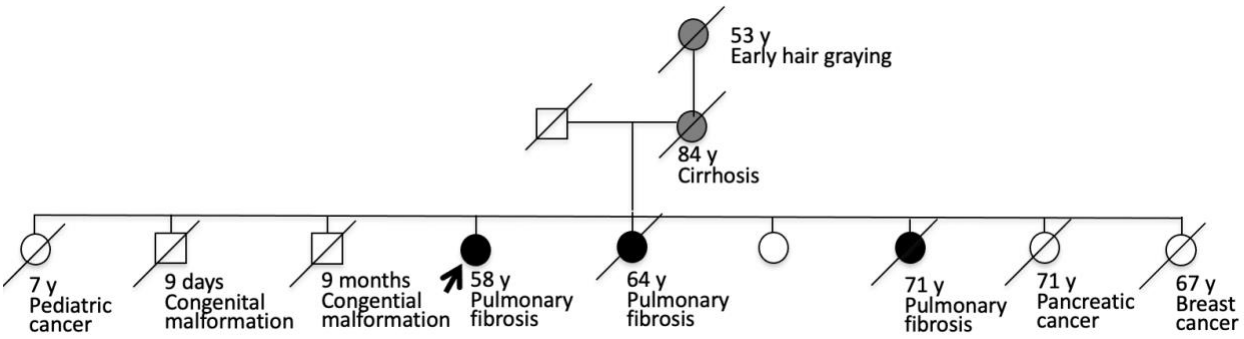

Supplemental Figure 2. P3 family pedigree. Pedigree of P3 displaying family members suffering from clinical features consistent with TBD/STS: early hair graying and cirrhosis in maternal grandmother and mother, respectively (grey shading); idiopathic pulmonary fibrosis in two sisters (black circles), both of whom passed away from pulmonary fibrosis associated complications at ages 64 and 71 years. Additionally, cancers resulting in death were reported in 3 sisters (unknown pediatric cancer occurrence in a 7-year-old, pancreatic cancer in a 71-year-old and breast cancer in a 67-year-old) and congenital malformations were noted in two brothers who passed away during infancy.

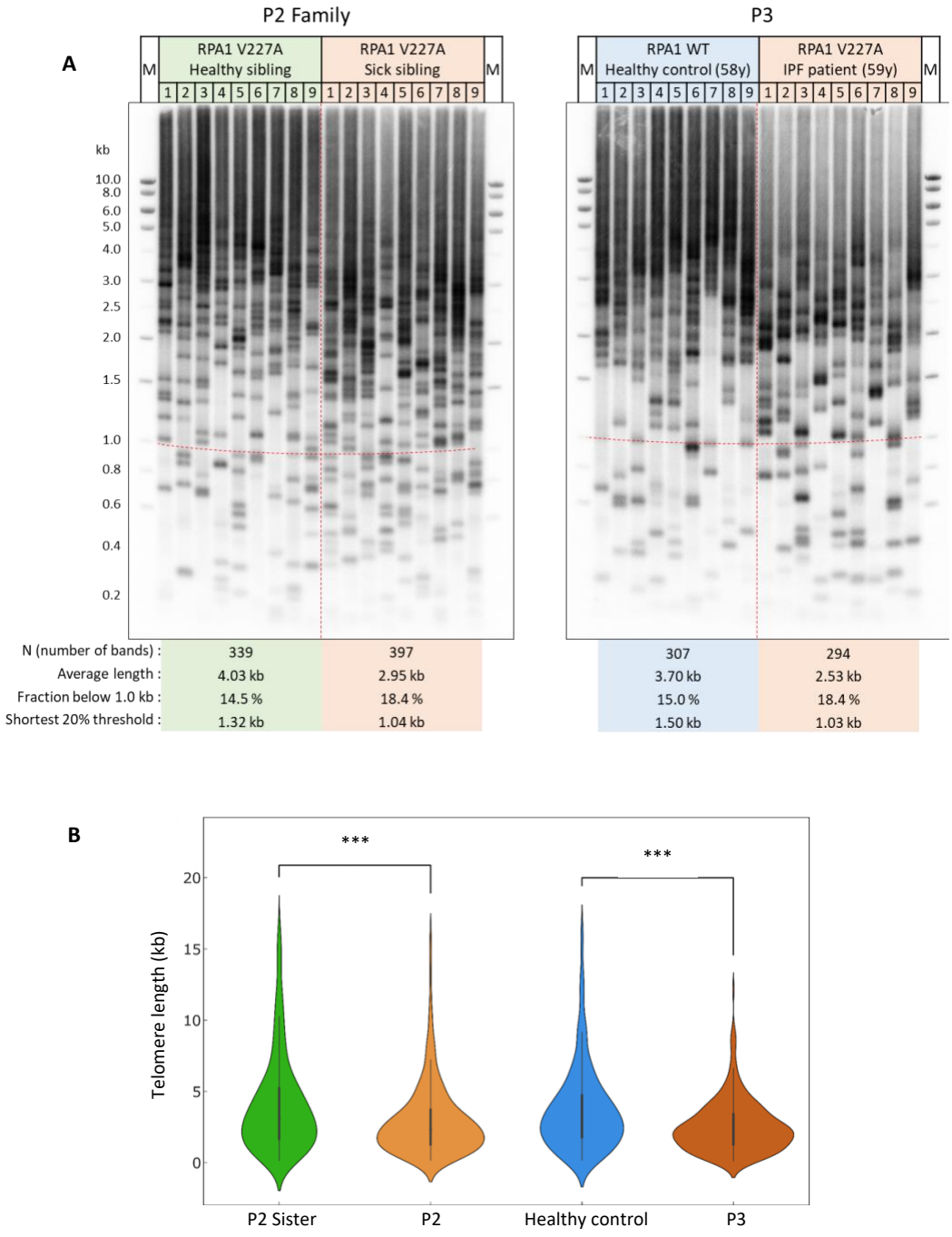

Supplemental Figure 3. A, Telomere Shortest Length Assay (TeSLA) reveals the length of individual telomeres from all chromosome ends in P2 and P3. Nine TeSLA PCRs were performed for each peripheral blood DNA sample obtained from clinically unaffected *RPA1* c.680T>C (V227A) carrier sister of P2 and P2 (left panel), in addition to the adult patient P3 and an age-matched control healthy individual (right panel). The characteristics of telomere length distributions are indicated below each blot. **B**, Violin plots of telomere length distribution obtained by TeSLA shows an increased fraction of very short telomeres (< 1 kb) in P2 and P3 compared to P2 sister and P3 age-matched control, respectively. A two-sided t-test for the differences between the means was performed, *** p<0.001.

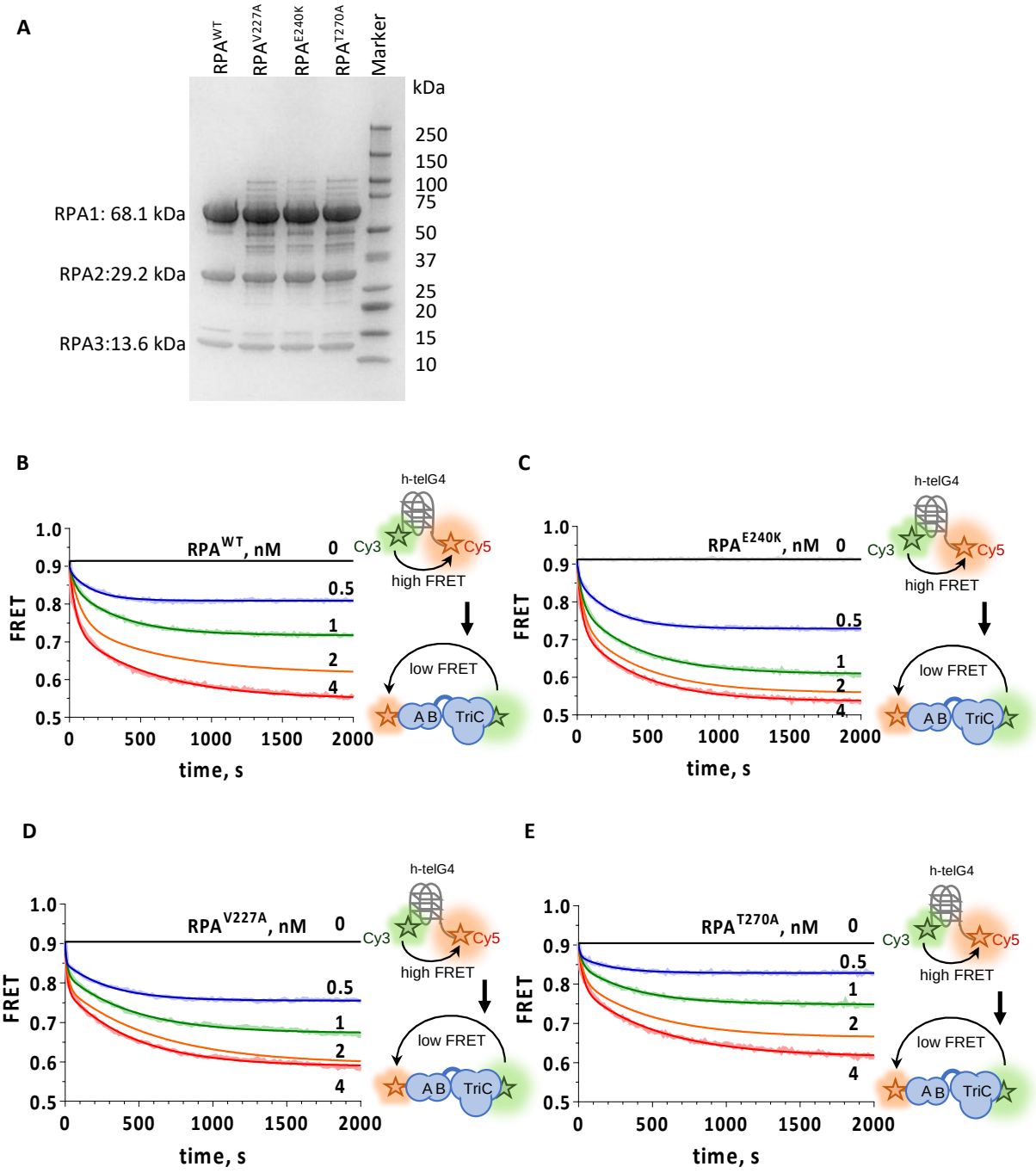

Supplemental Figure 4. RPA^{WT}, RPA^{V227A}, RPA^{E240K}, and RPA^{T270A} purification and time dependence of the telomeric G-quadruplex melting. A, Purified RPA^{WT}, RPA^{V227A}, RPA^{E240K}, and RPA^{T270A} protein complexes were analyzed by SDS-PAGE. Electrophoretic migration in a 10% acrylamide protein gel stained with Instant Blue Coomassie Protein Stain shows the presence of the three subunits of RPA (RPA1, RPA2 and RPA3) for all four proteins. **B-E,** Melting of the h-telG4 DNA, stabilized by the presence of 100 mM KCl at the indicated concentrations of RPA^{WT} (**B**), RPA^{E240K} (**c**), RPA^{V227K} (**D**) and RPA^{T270A} (**E**), shown for 1 of 3 representative experiments. Solid lines represent fitting of the data (dots) with two-phase exponential decay.

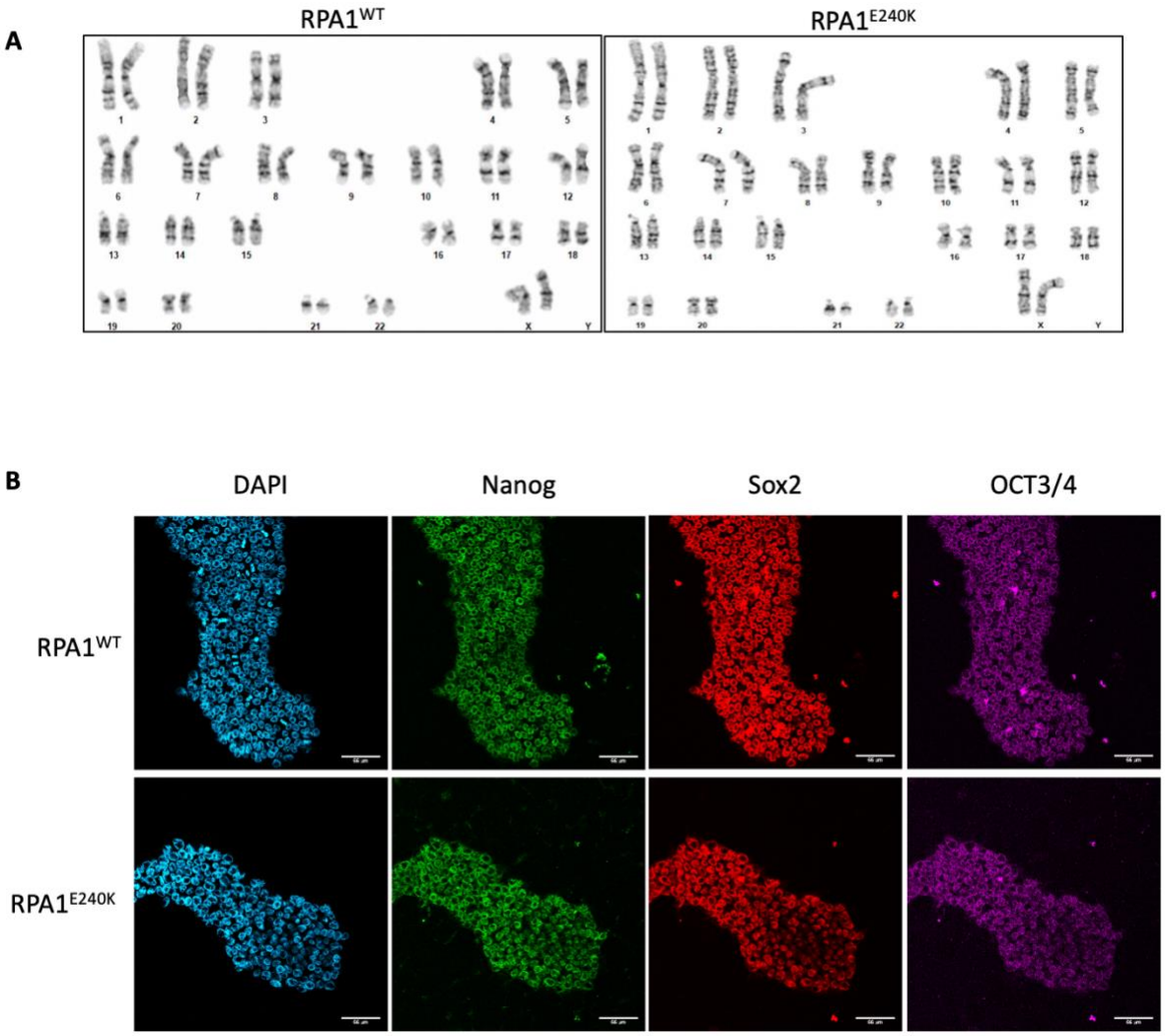

Supplemental Figure 5. Characterization of iPSC lines. A, Giemsa-banded metaphase chromosomes of RPA1^{WT} iPSC (left) and RPA1^{E240K} (right) iPSC. **B**, Representative immunofluorescence images of RPA1^{WT} (top row) and RPA1^{E240K} (bottom row) iPSC showing expression of pluripotency markers Nanog, Sox2 and Oct3/4 with DAPI used for nuclear stain. Total magnification 60x (scale bar: 66um).

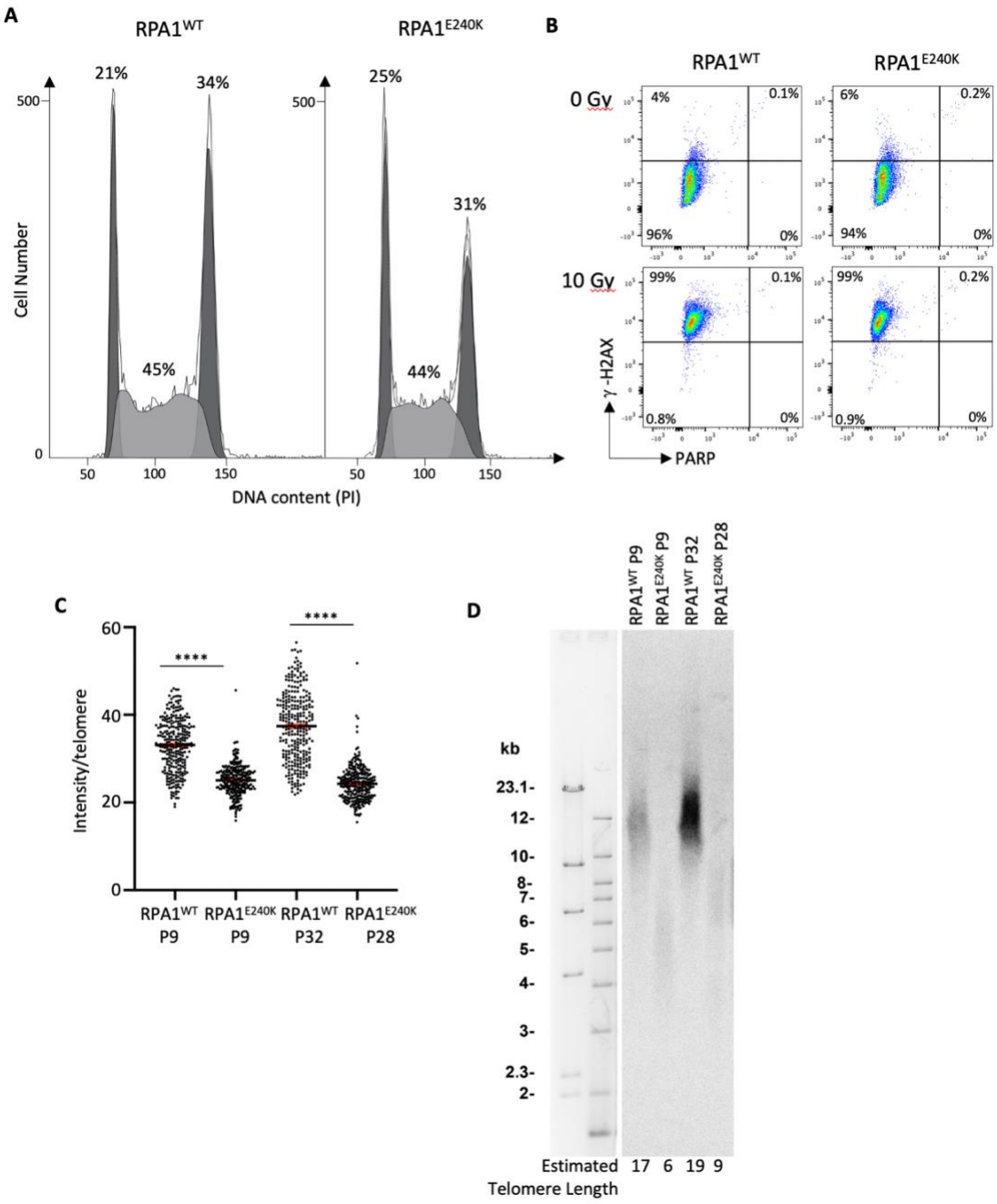

Supplemental Figure 6. Cell cycle, DNA damage response and telomere length at different passages in RPA1^{WT} and RPA1^{E240K} iPSC. **A**, Representative cell cycle profiles of RPA1^{WT} and RPA1^{E240K} iPSC analyzed by flow cytometry using propidium iodine (PI) stain. Cell proportions of G0/G1, S and G2/M phases at baseline are shown. **B**, Flow cytometric analysis of γ-H2AX and PARP cleavage in RPA1^{WT} and RPA1^{E240K} iPSCs at baseline (top plots) and 30 minutes following 10 Gy irradiation (bottom plots). Percentage of each population is denoted in each quadrant. **C**, Telomere length assessed in early and late passaged (P = passage) RPA1^{WT} and RPA1^{E240K} iPSCs using quantitative fluorescence in situ hybridization (Q-FISH). Spot analysis was performed on maximum intensity projections using custom FIJI macros based on local maxima detection. Approximately 300 interphase nuclei analyzed individually per sample. Graphs represent mean ± SEM of one of two independent experiments (two-sided unpaired t-test, ****p<0.0001). **D**, Telomere restriction fragment (TRF) analysis in early and late passaged RPA1^{WT} and RPA1^{E240K} iPSCs, digested with HinfI and RsaI enzymes followed by separation on 0.7% agarose gel.

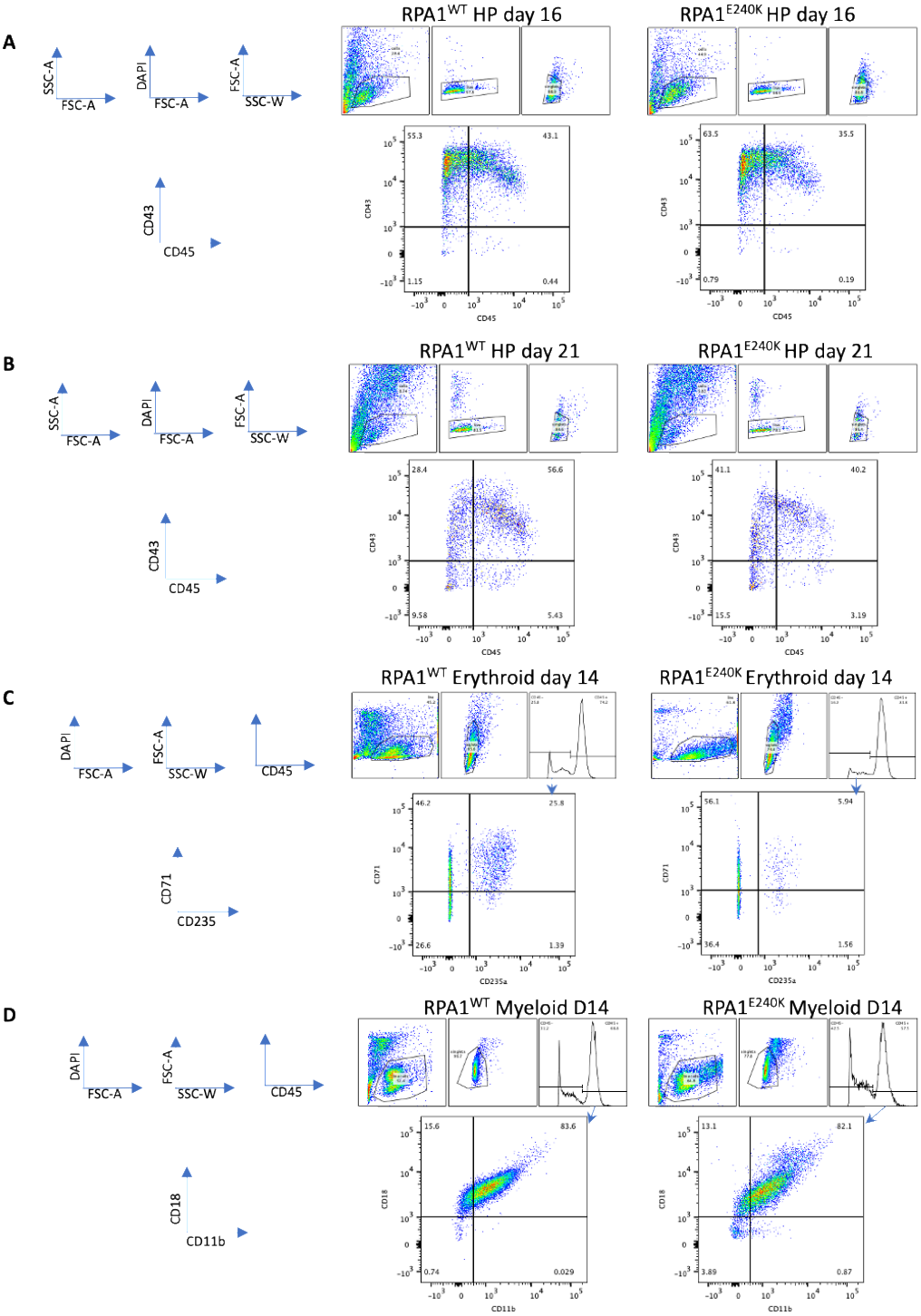

Supplemental Figure 7. Flow cytometry gating strategy for hematopoietic studies that assess HPs, erythroid and myeloid cells derived from RPA1^{WT} and RPA1^{E240K} iPSC. Gating strategy used for plots shown in main manuscript, Figure 3, is outlined for the analysis of hematopoietic progenitors (HP) at days 16 (**A**) and 21 (**B**), erythroid cells (**C**) and myeloid cells (**D**).

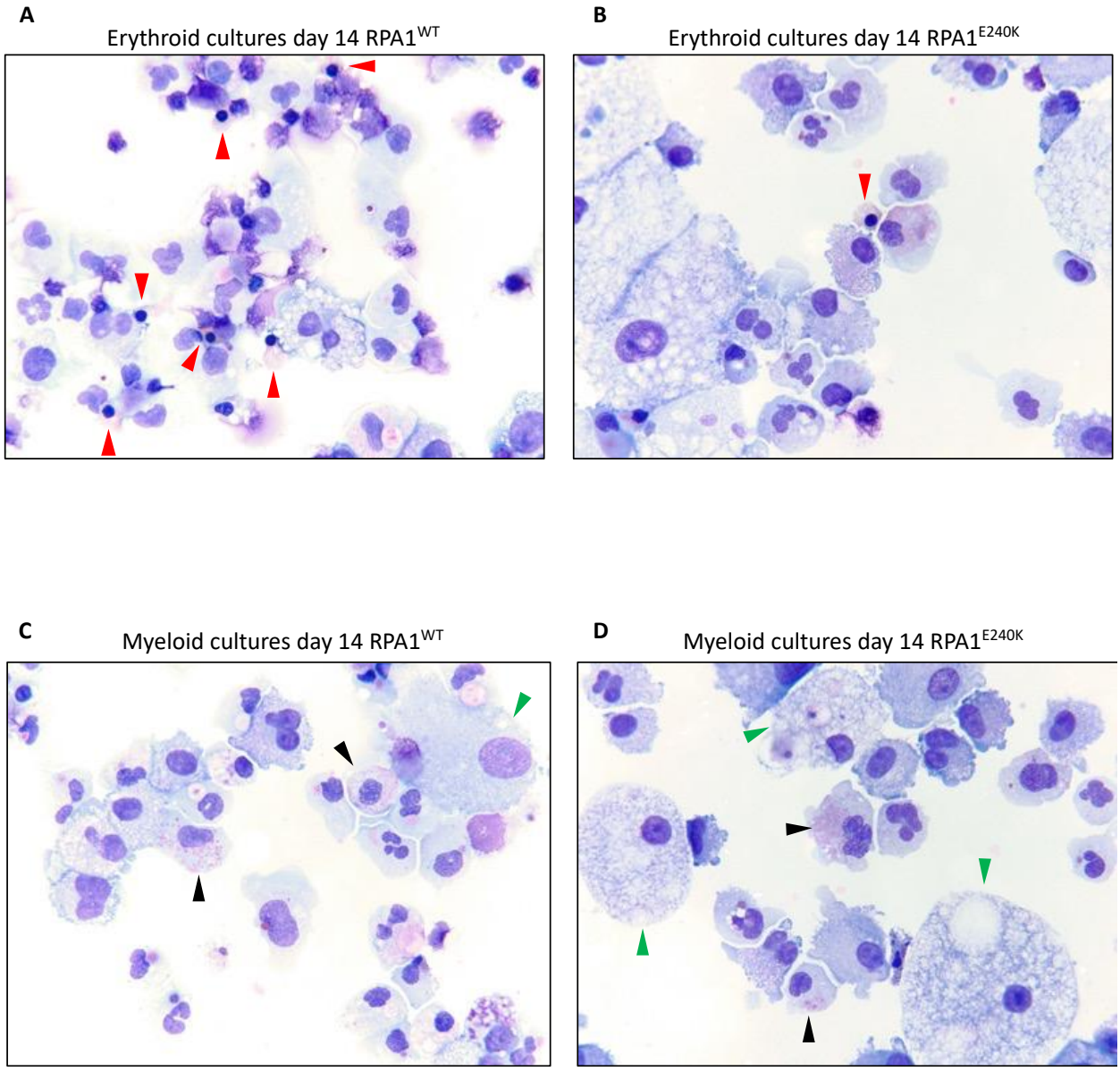

Supplemental Figure 8. Cytospin preparations of erythroid and myeloid cells derived from RPA1^{WT} and RPA1^{E240K} iPSC. A, Day 14 erythroid culture cytospins show several orthochromatic proerythroblasts indicated by red arrows in RPA1^{WT} compared to **B,** RPA1^{E240K} erythroid culture. Cytospin of myeloid cell cultures from **C,** RPA1^{WT} and **D**, RPA1^{E240K} on day 14 of differentiation. Myelomonocytic cells with maturing granulocytes are indicated by black arrows and macrophage-like cells by green arrows. All images are at 60x oil objective magnification.

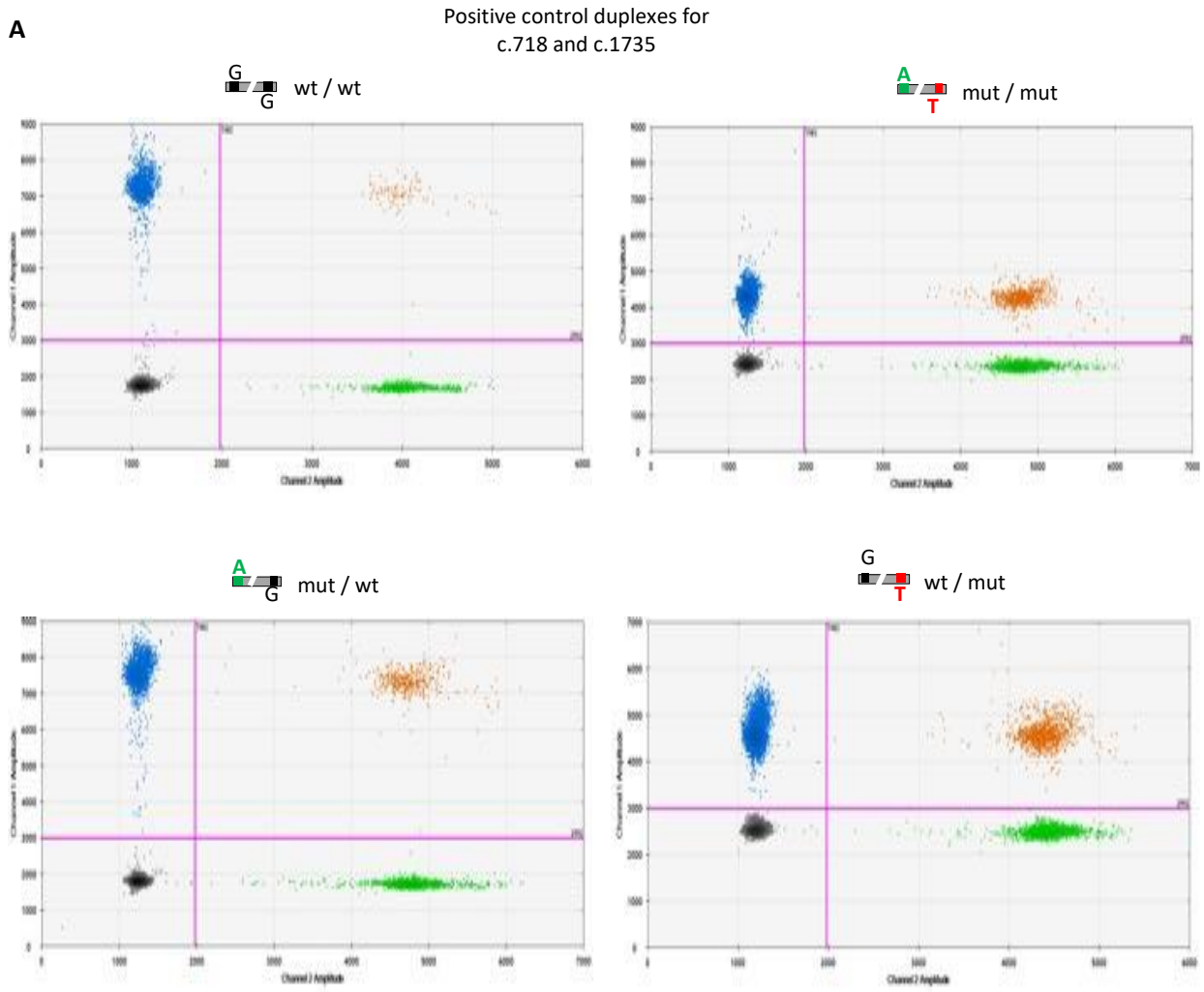

Supplemental Figure 9. Digital droplet (dd) PCR for haplotype phasing of *RPA1* germline (c.718) variant and somatic (c.1735) mutational positions in P1. A, Individual synthetic double-stranded DNA gene fragments (gBlocks) of *RPA1* gene containing either c.718G, c.718A, c.1735G, or c.1735T sequence permutations are used as control and emulsified in pairs (denoted as duplexes above each panel) into aqueous droplets with allele-specific fluorescence duplex probes (blue, c.718 position; and green, c.1735 position) for detection of alleles at two different loci. Following PCR, the droplets are positive for one fluorophore (blue or green), positive for both fluorophores (orange), or negative for both fluorophores (black). Positive controls for each duplex gBlock pair with respective probe is shown: top left panel shows wild type sequence at both c.718 (black, G) and c.1735 (black, G) positions labeled as (wt/wt); top right panel shows mutant sequences at both c.718 (green, A) and c.1735 (red, T) positions (mut/mut); bottom left panel shows mutant sequence at c.718 (green, A) and wild type sequence at c.1735 (black, G) position (mut/wt); bottom right panel shows wt sequence at c.718 (black, G) and mutant sequence at c.1735 (red, T) position (wt/mut).

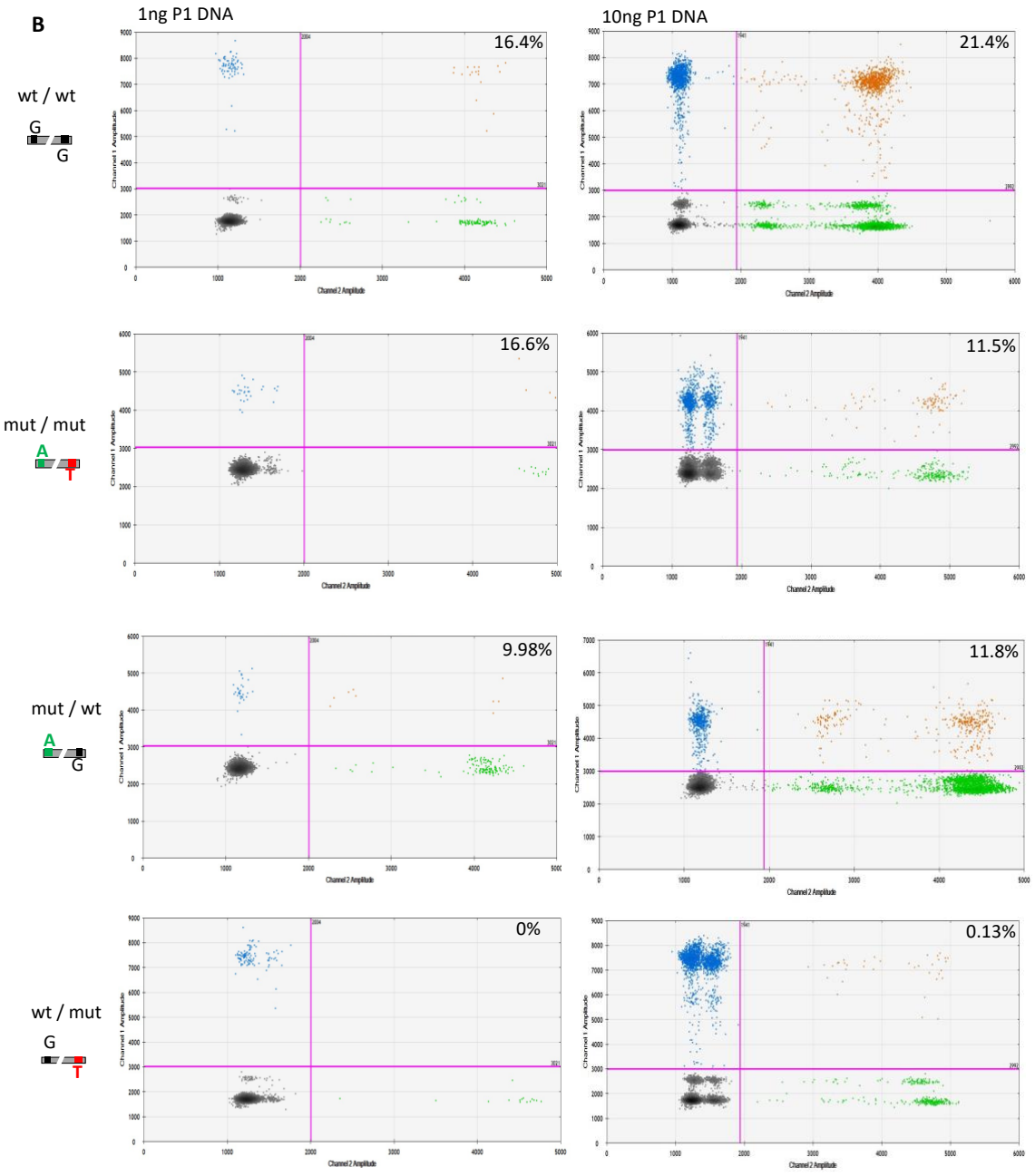

Continued: Supplemental Figure 9. Digital droplet (dd) PCR for haplotype phasing of *RPA1* germline (c.718) variant and somatic (c.1735) mutational positions in P1. B, DNA from peripheral blood of P1 collected at age 19 was diluted to 1ng (left column) and 10ng (right column) followed by emulsification into aqueous droplets (all samples with 16-20K droplets) together with allele-specific duplex probes. Cis-configured alleles co-segregate into the same droplets (orange, top right quadrant in all panels), because they are physically linked with co-partitioning greatly exceeding chance expectation. Trans-configured alleles partition independently into droplets (blue, top left; green, bottom right; all panels). Linked targets result in double-positive droplets in orange (top right quadrant in all panels). The percentage of linked targets in a sample was calculated by determining the excess of double-positive droplets over that expected due to chance colocalization of unlinked targets. Linkage was calculated using formula provided with value for linkage calculated by QuantaSoft Software in the table view as copies/µl of linked molecules for each well multiplied by 2 alleles which is divided by summation of total droplets of allele 1 and allele 2. Three linked haplotypes of c.718/c.1735 (germline/somatic) positions were identified above noise level: wt/wt, mut/mut and mut/wt, thus confirming cis configuration of the germline c.718A and somatic c.1735T alleles. Trans orientation of WT c.718G with mutant c.1735T was rejected based on 0% linkage in 1ng DNA. One of 2 independent experiments is shown.

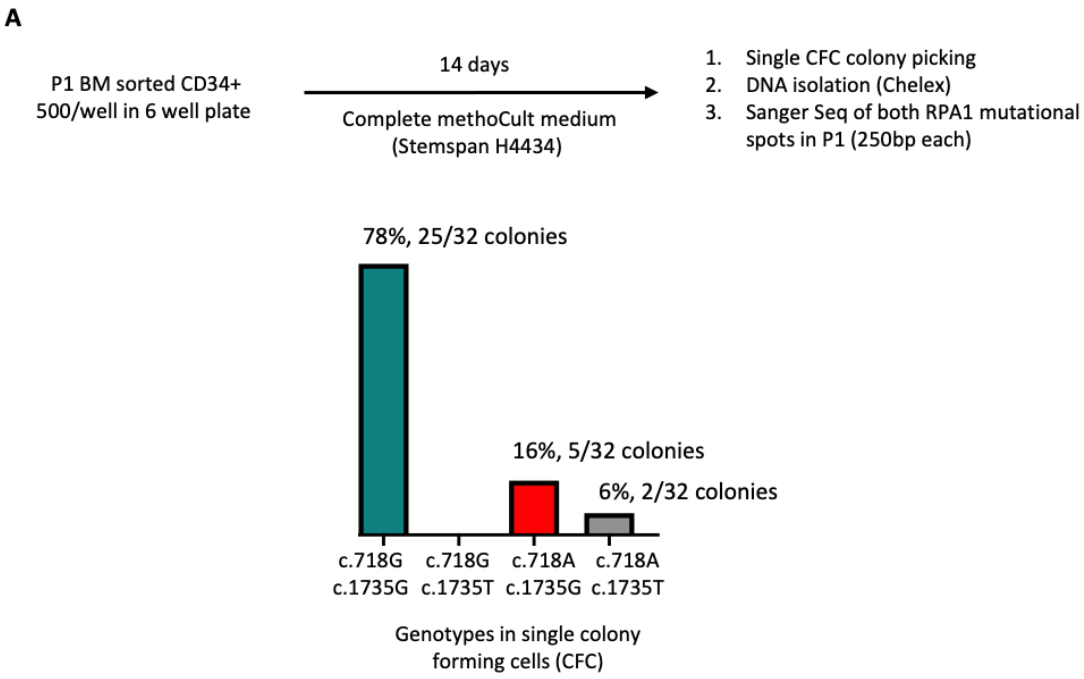

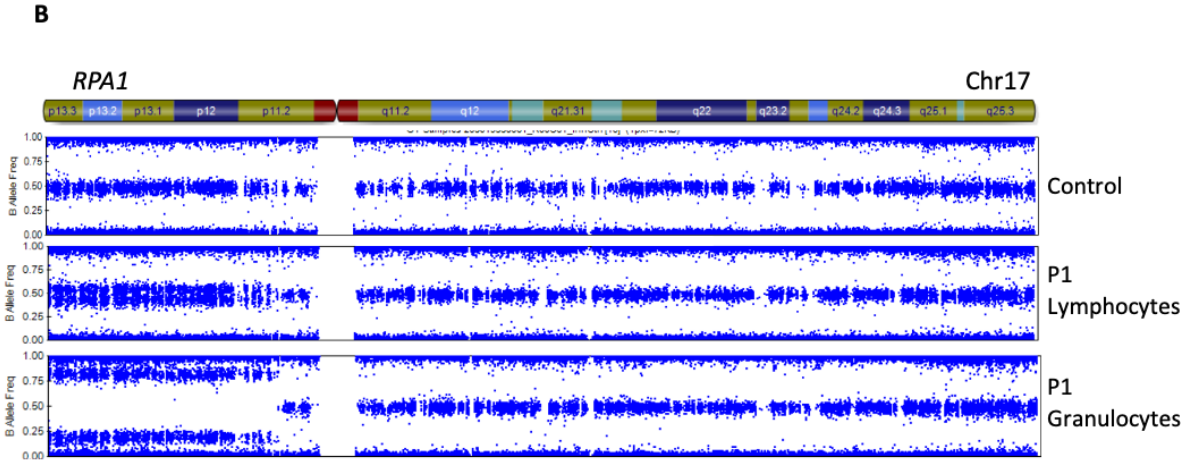

Supplemental Figure 10. P1 CD34⁺ single cell colony assay and SNP array analysis in lymphocytes and granulocytes. A, P1 bone marrow collected at age 20 years was FACS-sorted for CD34⁺ cells followed by seeding of 500 cells per well of a 6-well plate (total of 12 wells) for 14 days in semi-solid methylcellulose-based media. 88 single colonies were picked followed by DNA isolation and Sanger sequencing for both germline (c.718) and somatic (c.1735) positions. Successful analysis was achieved in 32 colonies revealing 3 independent clones: a major clone (78%, blue bar) with wt sequence at both positions (c.718G and c.1735G), corresponding to UPD17p rescue clone; a smaller clone (16%, red bar) with wt germline c.718G and wt c.1735G somatic positions, corresponding to native hematopoiesis; and a second rescue clone (6%, grey bar) positive for mutant sequences at both positions. **B**, Single nucleotide polymorphism (SNP) array analysis shown from control and P1 lymphocytes and granulocyte peripheral blood DNA collected at the age of 25 years. Allelic distribution of SNPs on chromosome 17 (encompassing *RPA1* locus) is depicted, with equal distribution of SNPs in control DNA while a small UPD17p clone was identified in lymphocytes compared to a large UPD17p clone in granulocytes from P1.

SUPPLEMENTAL TABLES

Pat. No.	Chr.	Genes	Variants		Exon	Protein Effect	VAF % (total depth)	CADD v1.6	gnomAD %AF v2.1.1 (AC/AN)	dbSNP#	ClinVar	Associated Germline Conditions (Inheritance Pattern)
P1	Chr17	***RPA1***	c.718G>A	p.E240K	9	Missense	24% (58)	23.3	Novel			none
	Chr13	*BORA*	c.227T>C	p.M76T	2	Missense	53% (17)	26.1	Novel			none
	Chr16	*CHTF18*	c.2014G>A	p.A672T	16	Missense	30% (20)	24.7	0.0047% (8/169576)	0.0047% (8/169576)		none
	Chr16	*ADAD2*	c.1498G>C	p.D500H	8	Missense	48% (23)	24.3				none
	Chr16	*CDH5*	c.1894G>T	p.G632C	12	Missense	49% (39)	24.5	0.0071%	rs759015093		none
	Chr22	*ZNF74*	c.220G>T	p.E74X	3	Stop-gain	48% (27)	23.5	0.0044%	rs568434993		none
	Chr12	*ANHX*	c.263C>T	p.P88L	3	Missense	64% (25)	24	0.0048%	rs1371589822		none
	Chr20	*ADRM1*	c.881C>T	p.S294L	7	Missense	60% (25)	29.1	0.0017%	rs747640477		none
	Chr11	*FAM160A2*	c.1075C>T	p.R359W	6	Missense	38% (34)	34	0.0018%	rs776133021		none
	Chr11	*ARL14EP*	c.458A>C	p.Q153P	3	Missense	52% (46)	24.3	0.0011%	rs766451036		none
	Chr16	*PDILT*	c.1250C>T	p.S417F	10	Missense	44% (68)	26.5	0.0004%	rs1234380634		none
	Chr17	*NGFR*	c.1255A>G	p.S419G	6	Missense	41% (22)	23.6	Novel			none
P2	Chr17	*UBTF*	c.1790T>C	p.S433P	13	Missense	60% (122)	24.7	Novel			Childhood-onset neuro-degeneration AD, E210K)
	Chr15	*TRIM69*	c.2263A>G	p.I445M	8	Missense	54% (220)	22.4	0.0004% (1/251352)	rs772259537		none
	Chr1	*NRAS*	c.289G>A	p.G12D *	2	Missense	45% (399)	25.7	0.0008% (2/251484)	rs121913237	Pathogenic[1,2]	Noonan syndrome (AD)
	Chr22	*MKL1*	c.1315A>C	p.I242L	10	Missense	41% (27)	24.4	Novel			Immunodeficiency (AR, homozygous K723X)
P4	Chr17	***RPA1***	c.808A>G	p.T270A	10	Missense	41% (51)	20.9	Novel			none

Supplemental Table 1. *De novo* nonsynonymous variants identified through family exome sequencing.
Filtering criteria are outlined in the methods. P3 not shown (due to lack of parental material). The non *de novo RPA1* mutations in P2 and P3 are depicted in Table 1.
Abbreviations: Chr, chromosome; VAF, variant allelic frequency; MAF, minor allelic frequency; AC, allele count; AN, allele number; n.a., not available.
*Confirmed as somatic (*NRAS*) or germline (RPA1) based on comparative sequencing of bone marrow and hair follicles.

Immunoglobulin	**3 weeks**	**6 months**	**1.75 years**	**6 months reference range** (mg/dL)	**1.75 years reference range** (mg/dL)
IgG	433[#]	177*	1,039[+]	218 - 907	345-1213
IgM	27.5	50.5	133.5	31 - 116	43-200
IgA	<6.0	7.9	NA	10 - 85	14-159
Cellular subsets	**3 weeks**		**1.75 years**	**6 months reference range** (mg/dL)	**1.75 years reference range** (mg/dL)
Lymphocytes	1,224*		1,300*	2.5-16.5	5.0-15.5
CD3+	832*		769*	1,920 - 4,991	1400-3700
CD3+CD4+	461*		499*	1,546 - 3,673	700-2200
CD3+CD8+	377		235	359 - 1,489	490-1300
CD19+	159*		234*	256 - 1,579	370-1400
CD3-CD56CD16+	245		191	116 - 783	130-720
Ratio, CD4:CD8	1.2*		2.1	1.7-4.8	0.9-4.4

Supplemental Table 2. Immunoglobulins and lymphocyte subsets over time in P4. [#]Immunoglobulin subsets at 3 weeks of age represent maternal transfer; [+]IgG replacement therapy. *Absolute subsets that are lower than the reference range.

Assay	**RPA^{WT}**	**RPA^{V227A}**	**RPA^{T270A}**	**RPA^{E240K}**
Binding stoichiometry to dT30 (Fig. 3b)[1]	2.27±0.06	1.34±0.03	1.59±0.04	1.10±0.03
K_d for dT15 (Fig. 3c)[2]	1.64±0.34 nM	0.79±0.14 nM (2.1-fold)	1.27±0.09 nM (1.3-fold)	0.21±0.02 nM (7.8-fold)
K_d for $(TTAGGG)_2TTA$ (Fig. 3d)[2]	0.67±0.07 nM	0.33±0.03 nM	0.84±0.08 nM	0.11±0.01 nM
h-telG4 melting extent at saturation (Fig. 3e)[3]	73±4%	71±2%	72±3%	86±4%
Apparent K_d from h-telG4 melting extent (Fig. 3e)[3]	0.40±0.09 nM	0.11±0.04 nM	0.78±0.11 nM	0.04±0.04 nM
h-telG4 melting rate at saturation (Fig. 3f)[3]	15.7±1.0pM/min	10.8±0.4pM/min	10.9±0.1pM/min	13.6±0.8pM/min
Apparent K_d from h-telG4 melting rate (Fig. 3f)[3]	1.16±0.21 nM	0.12±0.04 nM	0.59±0.03 nM	0.10±0.04 nM

Supplemental Table 3: Results of the FRET-based DNA binding and G-quadruplex melting experiments. [1]Binding stoichiometry X_0 values were calculated from the inflection points of the two-line linear regression fit of the FRET change upon binding of the respective protein to dT30 ssDNA (Figure 2b); the errors represent fitting uncertainty.
[2]The equilibrium dissociating constants were calculated by fitting the respective binding isotherms shown in figures 2c and 2d to a quadratic binding equation); the errors represent fitting uncertainty.
[3]The extents and rates of the h-telG4 unfolding were calculated using data shown in supplemental Fig. 4. The extents and rates were plotted as functions of protein concentration (Figure 2e and 2f) and fitted to a quadratic equation to yield apparent K_ds.

gDNA c.718 FWD	CCTGTGTTCAATCCCGCAGC
gDNA c.718 REV	TGACTTTAGAACTGACACCGCCT
gDNA c.1735 FWD	GAACAGGCATTTGAAGAAGTTTTCC
gDNA c.1735 REV	GTGCTGTTTGTCACCTACGG

Supplemental Table 4. RPA1 primers used for DNA Sanger and amplicon ultradeep sequencing.

cDNA c.718 FWD	GATCCGTACCTGGAGCAA
cDNA c.718 REV	CAGCTGTGAACTGCTTGTTA
cDNA c.1735 FWD	GCTGCTTATCTTGGGGAAT
cDNA c.1735 REV	CTCATGACCAGCCTTCG

Supplemental Table 5. **RPA1 primers used for RNA ultradeep sequencing.**

RPA1 c.718G>A, FWD	GAGCTACAGCTTTCAATAAGCAAGTCGACAAGTTCTTTCC
RPA1 c.718G>A, REV	GGAAAGAACTTGTCGACTTGCTTATTGAAAGCTGTAGCTC
RPA1 c.680T>C, FWD	GCTTTTCTCCCTAGAACTGGCTGACGAAAGTGGTGAAATCCG
RPA1 c.680T>C, REV	CGGATTTCACCACTTTCGTCAGCCAGTTCTAGGGAGAAAAGC
RPA1 c.808A>G, FWD	CCTGAAGATTGCTAACAAGCAGTTCGCAGCTGTTAAAAATGACTACGAG
RPA1 c.808A>G, REV	CTCGTAGTCATTTTTAACAGCTGCGAACTGCTTGTTAGCAATCTTCAGG

Supplemental Table 6. Primers used for mutagenesis of RPA1 in pET11d-human RPA construct.

Antibody	Catalog no.	Clone no.
anti-CD34-PE	550761	563
anti-CD43-APC	560198	IG10
anti-CD45-PE	555483	HI30
anti- CD235-FITC	559943	GA-R2 (HIR2)
anti-CD71-BV711	563767	M-A712
anti-CD11b-Alexa700	557918	ICRF44
anti-CD18-APC	551060	6.7

Supplemental Table 7. Flow cytometric antibodies.

SUPPLEMENTAL METHODS

Genomic studies in patients

DNA and RNA isolation

Genomic DNA was extracted from granulocytes or mononuclear cells obtained from peripheral blood (PB) or bone marrow (BM), or from skin-derived cultured fibroblasts using the QIAamp DNA Blood Mini Kit (Qiagen, cat no. 51104). RNA was extracted using Zymo Direct-Zol RNA microprep kit (ZymoResearch, cat no. R2063). RNA was reverse transcribed to cDNA with oligo(dT) primer and the SuperScript III RT–PCR kit (Thermo Fisher Scientific, cat no. 12574018).

Sanger sequencing

Primers flanking *RPA1* at positions c.718 and c.1735 were used to validate the ES results for germline variant c.718G>A and somatic mutation c.1735G>T in P1 using germline (fibroblast) and somatic (blood) DNA. The targets were amplified using Amplitaq Gold 360 DNA polymerase (Thermo Fisher Scientific, cat no. 4398813) with the following thermocycling conditions: 1 cycle of 95^{o}C for 10 minutes; 17 cycles of 95^{o}C for 50 seconds, 60^{o}C* (*decrease 0.5^{o}C each step) for 30 seconds and 72^{o}C for 30 seconds; 19 cycles of 95^{o}C for 50 seconds, 54^{o}C for 30 seconds followed by 72^{o}C for 45 seconds The purified PCR products were then bidirectionally sequenced on 3730XL DNA Analyzer (Applied Biosystems) and visualized using CodonCode Aligner v6.0.2 (Codon Code Corporation). Primer sequences provided in Supplemental Table 4.

Assessment of germline variant status

RPA1 germline status was ascertained by sequencing of skin-derived fibroblasts in P1, hair follicles in P2, and based on VAF in the germline range (~50%) in the absence of a clonal blood disease in P3 and P4.

RNA sequencing

Ribo-depleted RNA from P1 BM was sequenced on Illumina HiSeq platform with 75bp-paired end reads followed by data processing by St. Jude institutional automapper pipeline. Briefly the raw reads were first trimmed (Trim-Galore version 0.60), mapped to human genome assembly (GRCh37/hg19) (STAR v2.7) and then the gene level values were quantified (RSEM v1.31) based on GENCODE annotation (v19). Low count genes were removed from analysis using a cutoff of 10 reads with confident gene annotation of level 1 and 2 and protein-coding genes are used for differential gene expression (DGE) analysis. The individualized differentially expressed genes (iDEG) method was used for single-subject DGE analysis [3]. The parameters in iDEG were set as default except estimated Baseline= T. The significantly up- and down-regulated genes were defined by the thresholds as local FDR < 0.05 and fold change > 2^3. Primer sequences provided in Supplemental Table 5.

RPA1 allelic quantification of genomic DNA and cDNA using ultra deep sequencing in P1

Target enrichment for germline (*RPA1* c.718G>A) and somatic (*RPA1* c.1735G>T) mutations for P1 on genomic DNA or cDNA was performed using PCR enrichment followed by library preparation with NEBNext Ultra II DNA library prep kit (New England BioLabs, cat no. E7645S/L, E7600S) per manufacturer's instructions. Samples were sequenced on an Illumina HiSeq 2500 with 2 × 150 bp reads with a median

depth of 20,000 reads per sample. TrimGalore read trimming tool was used to remove adapter sequences and bases with low sequencing quality Following trimming, the resulting reads were aligned to the GRCh37/hg19 reference genome with BWA-MEM followed by indel realignment, duplicate removal, and SNP/INDEL calling using Freebayes with standard filtering parameters. Primer sequences provided in Supplemental Table 4.

Haplotype phasing using digital droplet (dd) PCR

No dUTP ddPCR supermix (Bio-Rad Laboratories, cat no. 1863024) was used for all experiments. Primers and probes were designed to amplify the germline *RPA1* c.718 and somatic *RPA1* c.1735 genomic positions. Primers and probes were used at concentrations of 900 nM and 250 nM, respectively with water (negative control), duplex G-blocks (positive controls) and 1ng or 10ng genomic DNA from P1 at age 19. Droplets were generated using the QX200 AutoDG Droplet Generator (Bio-Rad Laboratories), sealed with a pierceable foil heat seal (Bio-Rad Laboratories), and cycled in a C1000 Thermal Cycler (Bio-Rad Laboratories). Optimal cycling reactions were established using a gradient protocol. Final protocol used: 95°C, 10 min for 1 cycle; (94°C, 30 sec; 55°C, 1 min) for 40 cycles; 98°C, 10 min for 1 cycle. Droplets were read using a QX200 Droplet Reader (Bio-Rad Laboratories, cat no. 1864003) and data were analyzed using QuantaSoft Software v.1.7.4.0917 (Bio-Rad Laboratories). Linked targets result in double-positive droplets. The percentage of linked targets in a sample was calculated by determining the excess of double-positive droplets over that expected due to chance colocalization of unlinked targets. Linkage was calculated by QuantaSoft Software in the Table view as copies/µl of linked molecules for each well, according to previously established method for linkage calculation[4].

Quantification of uniparental isodisomy (UPD) 17p using single nucleotide polymorphism (SNP) array

DNA from granulocyte and lymphocyte fractions purified from PB of P1 and from a healthy control were genotyped using the human Infinium Omni2.5Exome-8 version 1.4 beadchip (Illumina, cat no. 20037367). Results were analyzed and visualized using the genome viewer in Illumina GenomeStudio software 2.0 (Illumina).

Single cell (sc) DNA and protein sequencing library preparation and sequencing

Single cell DNA sequencing with antibody-oligonucleotide staining was performed using the Tapestri single-cell DNA sequencing V2 platform, per manufacturer's instructions (MissionBio). Briefly, a custom targeted scDNA panel was designed and manufactured by MissionBio to amplify 298 amplicons including RPA*1* variants found in P1: germline c.718G>A (chr17:1782314:G>A) and somatic c.1735G>T (*RPA1*:chr17:1798378:G>T) with oligonucleotide-conjugated antibodies (AOC) targeting cell surface proteins of interest. Cryopreserved BM samples from P1 were thawed, washed with RPMI and quantified using a Cellometer Auto T4 (Nexcelom Bioscience). 1.0×10^6 viable cells were then resuspended in phosphate buffered saline (PBS, Gibco) and incubated with TruStain FcX, and 1X Tapestri staining buffer for 3 minutes at room temperature. The customized pool of 7 oligonucleotide-conjugated antibodies (CD3, CD11b, CD19, CD34, CD38, CD45RA, CD90) were then added and incubated for 30 minutes at room temperature. Following multiple washes with PBS supplemented with 5% fetal bovine serum (FBS; Gibco), cells were recounted, diluted to a concentration of 4,000,000 cells/mL in Tapestri cell buffer. Next, 50 µL of the cell suspension was loaded onto a microfluidics cartridge and cells were encapsulated on the

Tapestri instrument followed by the cell lysis and protease digestion in a thermal cycler within the individual droplet. The cell lysate was then barcoded such that each cell had a unique label. Amplification of the targeted DNA regions and antibody oligonucleotide tags was performed by a targeted PCR on the barcoded DNA emulsions. Emulsions were broken and DNA digested and purified with 0.7X Ampure XP beads (Beckman Coulter). The beads were pelleted, and the supernatant retained for antibody library preparation, while the remaining beads were washed with 80% ethanol and the DNA targets eluted in nuclease-free water. The supernatant containing the antibody tags was incubated with a biotinylated capture oligo (/5Biosg/CGAGATGACTACGCTACTCATGG/3C6/, Integrated DNA Technologies (IDT)) at 96°C for 5 min, followed by ice for 5 min, and recovered with streptavidin beads (Dynabead MyOne Streptavidin C1, Thermo Fisher Scientific). Indexed Illumina libraries were generated by amplifying DNA libraries with MissionBio V2 index primers and protein libraries bound to streptavidin beads with i5 and i7 index primers (IDT). All libraries were quantified using an Agilent Bioanalyzer and pooled for sequencing on an Illumina NovaSeq6000 with 150 base paired ending multiplexed runs. Adaptor sequence trimming, sequence read alignment to human genome (GRCh37/hg19), sequence read assignment to cell barcodes, and genotype calling with GATK were performed for all FASTQ files for single cell DNA libraries using Tapestri analysis pipeline. Using a loom file for subsequent processing, low quality genotypes or cells were filtered in Tapestri Insights v2.0 and Mosaic (https://github.com/MissionBio/mosaic), where a whitelist was used to filter out clones that did not have successful coverage for both *RPA1* c.718 and *RPA1* c.1735 positions within the same cell. We defined genetic clones based on their genotype status at both positions of interest.

Telomere length studies

Flow cytometry-based fluorescence in situ hybridization (Flow-FISH)

Telomere length analysis was done by flow-FISH as previously described[5]. Briefly, peripheral blood samples were stained with a telomere specific (CCCTAA)3-peptide nucleic acid (PNA) FITC labeled FISH probe (Panagene) for DNA hybridization, followed by DNA counterstaining with LDS 751 (Sigma). Lymphocytes and granulocytes were identified based on forward scatter and LDS 751 staining. All measurements were carried in triplicates and mean telomere length was calculated in kilobases (kb) in relation to the internal control (bovine thymocytes) with known telomere length. Healthy controls for calculation of the percentile curves were used as described previously[5].

Telomere Restriction Fragment (TRF) analysis using Southern blot

Genomic DNA (800ng-1000ng) extracted from peripheral blood cells of P2 and family, as well as P3 and age matched control, was digested with HinfI and RsaI enzymes, resolved by a 0.7% agarose gel, and transferred to a nylon membrane. Hybridization at 42°C for 16 hours was performed using EasyHyb solution (Roche) and γ-32P-labeled (TTAGGG)4 probe. After washes, membranes were exposed over a PhosphorImager (AGFA). PhosphorImager exposures of telomere-probed Southern blots were analyzed with the ImageJ program. The digitalized signal data were then transferred to Microsoft Excel and served as the basis for calculating mean TRF length using the formula L = (ODi)/(ODi/Li), where ODi = integrated signal intensity at position i and Li = length of DNA fragment in position as determined by DNA ladders (1kb plus lambda HindIII ladder, Invitrogen).

Quantitative fluorescence in situ hybridization (Q-FISH)

Telomere length in iPSC and HP was analyzed by Q-FISH as reported previously[6]. Briefly, 500,000 interphase cells/genotype were hybridized using the peptide nucleic acid–FISH method followed by telomere staining with FITC- labeled (CCCTAA)3 peptide nucleic acid (PNA) probe (Telomere PNA FISH kit/FITC, DAKO) and DAPI counterstain. 300 interphase nuclei from each sample were analyzed individually to enumerate fluorescence (spot intensity X spot area)/telomere using a Zeiss Axio Imager.Z2 using a Zeiss Plan-Apochromat 63x objective and Applied Spectral Imaging SpotScan software v8.1.1 (ASI) with fixed exposure times for all samples. Q-FISH analysis for telomere length in early and late passaged (P = passage) $RPA1^{WT}$ and $RPA1^{E240K}$ iPSCs was performed using Z-stack images acquired on a Zeiss 980 LSM with a 63x 1.40 NA oil objective, using the same settings for all samples. Spot analysis was performed on maximum intensity projections using custom FIJI macros based on local maxima detection (code available upon request).

Telomere Shortest Length Assay (TeSLA)

TeSLA was performed as previously described by Lai et al.[7]. Briefly, an equimolar mixture (50 pM each) of the six TeSLA-T oligonucleotides (containing seven nucleotides of telomeric C-rich repeats at the 3' end and 22 nucleotides of the unique sequence at the 5' end) was annealed to and ligated with 50 ng of undigested genomic DNA at 35°C for 14 h. Then, genomic DNA was digested with *Cvi*AII, *Bfa*I, *Nde*I, and *Mse*I, the restriction enzymes that create short either AT or TA overhangs. Digested DNA was then treated with Shrimp Alkaline Phosphatase to remove 5' phosphate from the DNA fragments to avoid their ligation to each other during the subsequent step. Upon heat-inactivation of phosphatase, partially double-stranded AT and TA adapters were added (final concentration 1 µM each) and ligated to the dephosphorylated fragments of genomic DNA at 16°C overnight. Following ligation of the adapters, genomic DNA was diluted to a final concentration of 20 pg/µL, and 2-4 µL of it was used in a 25 µL PCR reaction to amplify terminal fragments using primers complementary to the unique sequences at the 5' ends of the TeSLA-T oligonucleotides and the AT/TA adapters. FailSafe polymerase mix (Epicenter) with 1× FailSafe buffer H was used to efficiently amplify G-rich telomeric sequences. Entire PCR reactions were then loaded onto the 0.9% agarose gel for separation of the amplified fragments. To specifically visualize telomeric fragments, the DNA was transferred from the gel onto the nylon membrane by Southern blotting procedure and hybridized with the ^{32}P-labeled $(CCCTAA)_3$ probe. The sizes of the telomeric fragments were quantified using TeSLA Quant software[7].

RPA biochemical studies

Expression and purification of wild type and mutant RPA

Site-directed mutagenesis (Agilent) was performed with custom synthesized primers (IDT) to introduce *RPA1* c.680T>C, p.V227A and *RPA1* c.718G>A, p.E240K and *RPA1* c.808A>G, p.T270A variants independently into pET11d-Human RPA construct to yield RPA^{V227A}, RPA^{E240K} and RPA^{T270A} respectively[8]. The presence of the mutation was confirmed by sequencing. Both wild type and mutant proteins were expressed and purified as previously described[8]. Primer sequences provided in Supplemental Table 6.

FRET-based ssDNA binding assays

FRET-based assays were used to monitor RPA^{WT}, RPA^{V227A} and RPA^{E240K}, and RPA^{T270A} binding to ssDNA dually labeled with Cy3 and Cy5 fluorophores, as previously described[9]. All DNA oligonucleotides were

purchased from Integrated DNA Technologies (Coralville, IA, USA). The reactions were carried out using Cary Eclipse Fluorimeter (Agilent). Cy3 (FRET donor) dye was excited at 530 nm. Emission of the acceptor Cy5 and donor Cy3 fluorophores was monitored simultaneously at 660 nm and 565 nm, respectively. Excitation and emission slit widths were all set to 10 nm. Poly-dT ssDNA binding experiments were carried out in the reaction buffer containing 30 mM HEPES-KOH, pH 7.5, 5 mM Mg-acetate, 150 mM NaCl and 1 mM DTT, at 37 °C. Binding to the unfolded human telomeric (h-telG4) DNA sequence (Cy5-$(TTAGGG)_5$-Cy3) was carried out in the reaction buffer containing of 30 mM HEPES-KOH, pH 7.5, 100 mM LiCl and 1 mM DTT. Note that h-telG4 binding experiments were only used to determine the maximum extension of this ssDNA and the FRET value to be used to indicate 100% unfolded h-telG4 in the G4 melting experiments described below. This is because the RPA^{V227A}, RPA^{T270A} mutants are sensitive to LiCl (not shown). After the baseline of buffer only was recorded, the Cy5-$(dT)_{30}$-Cy3, Cy5-$(dT)_{15}$-Cy3, or Cy5-TTAGGGTTAGGGTTA-Cy3 (1 nM) was added to the reaction mixture followed by addition of indicated concentrations of the wild type or mutant RPA. FRET efficiency was calculated as $FRET = \frac{4.2*I_{Cy5}}{4.2*I_{Cy5}+1.7*I_{Cy3}}$, where I_{Cy5} is the averaged acceptor intensity and I_{Cy3} is the averaged donor intensity after subtracting the background fluorescence[9]. The calculated FRET efficiency was plotted against protein concentrations and analyzed using GraphPad Prism software. Stoichiometric binding curves (dT30 ssDNA) were fitted with two lines to determine the inflection point, and equilibrium binding curves (dT15 ssDNA) were fitted using quadratic binding equation to determine the Kds.

FRET-based G4 quadruplex melting assays

RPA-mediated melting of the folded h-telG4 DNA (Cy5-$(TTAGGG)_5$-Cy3) quadruplex was monitored in the reaction buffer containing 30 mM HEPES-KOH, pH 7.5, 1 mM DTT, 5 mM Mg-acetate and 100 mM KCl, which stabilizes the quadruplex[10]. For each RPA concentration, the averaged FRET efficiency from 3 different experiments was plotted against time and fitted to a double exponential whose combined amplitude was compared to baseline FRET efficiency value for Cy5-$(TTAGGG)_5$-Cy3 to determine the extent of h-telG4 melting. The initial rate of G4 melting was determined as the slope of the linear portion of the progress curve (10-40 s depending on the protein concentration) for each assay, divided by 0.38 (FRET efficiency difference between fully folded and fully stretched h-telG4 DNA) and multiplied by the total amount of DNA present (1 nM). Both the rate and extent of h-telG4 melting were plotted against protein concentration and analyzed using GraphPad Prism software.

Modeling and characterization of RPA1 p.E240K in iPSC

Generation, quality control and maintenance of human iPSC

ATCC normal adult human primary dermal fibroblasts (PCS-201-012) were reprogrammed into iPSC using the integration-free CytoTune2.0 Sendai virus reprogramming kit (Thermo Fisher Scientific Fisher, cat no. A16517) following methods previously reported [11,12]. G-banding karyotype was performed in all cell lines prior to experiments and pluripotency was confirmed in iPSC using flow cytometric analysis for SSEA-4 stem cell surface marker as previously described[13]. iPSC were maintained on 6-well tissue culture plates thinly coated with Matrigel® (Corning, cat no. 354230) in cGMP, feeder-free maintenance mTeSR1 medium (Stem cell Technologies, cat no. 85850). Culture medium was changed daily and iPSC were split every three to four days. Briefly, medium was aspirated, and wells were sequentially washed with PBS (Gibco) followed by cell dissociation in ReLeSR (Stem Cell Technologies, cat no. 05872) for 3 min. 1 mL

mTeSR1 medium containing 1.25 µM ROCK inhibitor (Sigma, cat no. Y0503) administered per well and cells were pipetted 3–4 times using a 5 mL serological pipette to dissociate into small to medium sized clusters and split onto new 6-well plates.

RPA1 editing in iPSC using CRISPR/Cas9 system

Human *RPA1*_E240K_PCS201 iPSC Clone 1 was generated using CRISPR-Cas9. Briefly, PCS201 iPSC were pretreated with StemFlex (Thermo Fisher Scientific Fisher, cat no. A334901) supplemented with 1X RevitaCell (Thermo Fisher Scientific Fishe, cat no. A2644501) for 1 hour. Approximately $1X10^6$ cells were transiently co-transfected with precomplexed ribonuclear proteins (RNPs) consisting of 500 pmol of chemically modified sgRNA (SS125.*RPA1*.g7-5' GCUCAUUGAAAGCUGUAGCU-3', Synthego), 140 pmol of *sp*Cas9 protein (St. Jude Protein Production Core), 3ug of ssODN donor (SS125.h*RPA1*.g7.anti.ssODN5'ctaaagtcagcacggccataccttgttcacttcaataagaggaaagaacttgtccacttgTtTattgaaa gctgtagctcggatttcaccctgcagaagcacgtgggcaggttagggctgcgggattgaacacaggccaccc3', IDT) and 1ug of pMaxGFP (Lonza, cat no. 1040). The transfection was performed via nucleofection (Lonza, 4D-Nucleofector™ X-unit, cat no. AAF-1002X) using solution P3 and program CA-137 in a large (100ul) cuvette according to the manufacturer's recommended protocol. Five days post-transfections, cells were sorted for GFP+ (transfected) cells and plated onto Vitronectin XF (Stem Cell Technologies, cat no. 07180) coated plates into prewarmed (37C) StemFlex media supplemented with 1X CloneR (Stem Cell Technologies, cat no. 05888). Clones were screened and verified for the desired modification via targeted deep sequencing using gene specific primers with partial Illumina adapter overhangs (SS125.F – 5'-ACCCTGTTTGTGCAAGGGCCACTGC-3' and SS125.R – 5'-GCCAAGCCACAGAACCTGAGACTACCA-3', overhangs not shown) on a Miseq Illumina sequencer. NGS analysis of clones was performed using CRIS.py[14]. *RPA1* whole gene sequencing was performed in iPSC to rule out off-target mutations introduced during CRISPR/Cas9 manipulation as well as second site mutations acquired in the process of culturing. Genomic DNA libraries from all iPSC cell lines were prepared by enzymatic gDNA fragmentation (Twist Bioscience, cat no. 101058), Twist universal adapter ligation followed by PCR amplification (Twist Bioscience, cat no. 101058 custom *RPA1* gene panel), purification (Twist Bioscience, cat no. 101058) and quality control analysis using 2100 BioAnalyzer High Sensitivity kit (Agilent) by manufacturer's instructions. Samples were sequenced on an Illumina HiSeq 2500 with 2 × 150 bp reads. Low quality reads and adapters were trimmed using TrimGalore. Following trimming, the resulting reads were aligned to the GRCh37/hg19 reference genome with BWA-MEM followed by indel realignment, duplicate removal, and SNP/INDEL calling using Freebayes with standard filtering parameters.

Assessment of iPSC pluripotency state by immunofluorescence

Immunofluorescence analyses of undifferentiated human iPSCs in monolayer culture was performed. For this purpose, cells were fixed 10 min at room temperature with 4% paraformaldehyde (Sigma-Aldrich) and washed twice with PBS. Cells were blocked for 1 hour at room temperature with 0.1% Triton (Sigma-Aldrich), 10% FBS (Sigma-Aldrich) and 1% BSA (Sigma-Aldrich) for 15 min. Primary antibodies diluted in Triton block solution were added and incubated for 3 hours at room temperature. Thereafter, cells were washed with PBS and secondary antibodies in Triton block were added for one-hour incubation in the dark. Slides were washed with PBS and mounted using vectashield containing DAPI (Biocompare, cat no. H1200) followed by applying coverslip. All samples were imaged the following day using Zeiss LSM 980 confocal scanning microscope (Zeiss). Primary antibodies used were Nanog (NL493, R&D systems, cat

NL1997G), Oct-3/4 (AF647, Novus bio. cat no IC1759R-100UG), Sox2 (AF594, Novus bio. cat no IC2018T-100UG). Supplemental Table 7 provides all antibodies used with clone and catalog numbers.

Immunoblotting of RPA1 in iPSC

iPSCs were washed with PBS and collected in RIPA lysis buffer (Thermo Fisher Scientific Fisher, cat no. 89900) containing protease and phosphatase inhibitors (Thermo Fisher Scientific Fisher, cat no. A32959). Lysates were quantified using Qubit 4 fluorometer (Thermo Fisher Scientific Fisher Scientific). Proteins were separated by SDS–PAGE, electro transferred to polyvinylidene difluoride membranes, and blocked for 1 h at room temperature with 5% nonfat dry milk in Tris-buffered saline (TBS) containing 0.5% Tween 20 (Amresco: 0777-1L) (TBST). Membranes were washed and incubated overnight at 4 °C with anti-RPA1 primary antibody (Cell signaling, cat no. 2267, dilution 1:1,000) with anti-β-actin (Cell signaling, cat no. 4970, dilution 1:10,000) used as a loading control. Membranes were washed with TBST and incubated with horseradish peroxidase (HRP)- conjugated anti–rabbit IgG secondary antibody (Cell signaling, cat no. 7074S, dilution 1:5,000) for 1 h at room temperature. Immunoreactive material was revealed using Amersham ECL prime detection (Amersham Biosciences, cat no. RNP2232) and the ChemiDoc touch imaging system (Bio-Rad Laboratories).

Preparation and analysis for DNA content

iPSC samples were washed once with PBS, centrifuged, and the supernatant decanted. Cell were resuspended in 1ml of a hypotonic solution containing propidium iodide (PI) (0.05 mg/ml PI, 0.1% w/v sodium citrate, 0.1% v/v Triton X-100). DNAse-free RNAse (ribonuclease A 0.2mg/ml in 10mM Tris-HCl/pH 7.5/15mM NaCl) was added (10ul/sample) followed by incubation at room temperature for 30 minutes. Samples were analyzed using a BD Biosciences Fortessa analyzer, collecting data from 10,000 single cells. The percentages of cells in the different phases of the cell cycle were determined using ModFit software (Verity Software House).

Apoptosis and DNA damage assessment at baseline and following DNA damage

iPSCs were seeded at 70% confluency and the following day cells were either untreated or treated with 10Gy radiation (Gammacell 40, Best Theratronics) and then allowed to recover for 30 mins. g-H2AX and cleaved PARP were measured in these samples per Apoptosis and DNA damage kit (BD Biosciences, cat no. 562253). Briefly, 1×10^6 un- and treated cells were fixed and permeabilized with BD Cytofix/Cytoperm Fixation/Permeabilization solution for 30 min at room temperature followed by additional permeabilization and fixation. Cells were washed with BD Perm/Wash Buffer and stained with AF647 mouse anti-H2AX (pS139) (BD Biosciences, cat no. 51-9007683,) and PE mouse anti-cleaved PARP (Asp214) antibody (BD Biosciences, cat no. 51-9007684) for 20 min at room temperature. The stained and washed cells were resuspended in 500 µL PBS and analyzed with a flow cytometer (Cantos II flow cytometer, Becton Dickinson). Data were analyzed using FlowJo software (FlowJo v10).

Hematopoietic differentiation of induced pluripotent stem cells (iPSCs)

Generation of iPSC line using CRISPR/Cas9 editing, cell culture, quality assessment and iPSC characterization studies are described in supplemental methods. iPSCs were differentiated for 21 days using the STEMdiff Hematopoietic Kit (Stem Cell Technologies, cat no. 05310) as previously described[15]. One day prior to differentiation, a total of 45–75 iPSC clusters (4-8 single cells per cluster) were seeded

per well into a Matrigel-coated six-well plate and cultured overnight. On day zero of differentiation, medium A was added to promote mesodermal differentiation and half-medium A change was done on day two. Supernatant was removed on day three and hematopoietic differentiation medium B was added, followed by half-medium change on days five, seven, 10, 12, 14, 17, and 19. Full supernatant was harvested on days 16 and 21 for flow cytometric analysis of pan-hematopoietic markers (CD43, CD45). For erythroid and myeloid terminal differentiation, day 10 hematopoietic progenitors (HP) were flow-sorted (BD FACS Aria, Becton Dickinson) based on CD43 and CD34 expression and 30,000 cells in triplicates were seeded for erythroid differentiation (Stem Cell Technologies, cat no. 02692; EPO, IL-3, and SCF) and myeloid differentiation (Stem Cell Technologies, cat no. 02693; G-CSF, GM-CSF, SCF, and TPO) in StemSpan SFEM II hematopoietic cell expansion media (Stem Cell Technologies, cat no. 09655). Following 14-day differentiation, erythroid ($CD45^{-}CD71^{+}CD235^{+}$) and myeloid cells ($CD45^{+}CD18^{+}CD11b^{+}$) were counted using Cellometer Auto T4 (Nexcelom Bioscience) and stained with cell surface antibodies detailed in supplemental material for flow cytometric analysis.

Cytospin and Wright-Giemsa stain of myeloid and erythroid cells

Day 14 myeloid and erythroid cells from 1 well were centrifuged at 300rpm at room temperature followed by media aspiration and resuspension in phosphate buffered solution (PBS, Gibco). Separate cytofunnels were loaded with different cell populations and cytospun on a Thermo Fisher Scientific Cytospin 4 at 60 g for 5 minutes at room temperature. All slides were then Wright-Giemsa stained for microscopic imaging. Digital images were taken with a 60x oil objective and Olympus DP22 camera and scaled identically.

Statistical analysis

Data for all experiments from biological and technical replicates were presented as the mean values ± standard deviation (SD) or standard error of mean (SEM) as specified in each figure legend. Statistical significance was assessed using GraphPad Prism v 7.04 software employing paired and unpaired Student's *t* test. *P* values < 0.05 were considered statistically significant.

Members of the Undiagnosed Diseases Network

Maria T. Acosta
Margaret Adam
David R. Adams
Pankaj B. Agrawal
Justin Alvey
Laura Amendola
Ashley Andrews
Euan A. Ashley
Mahshid S. Azamian
Carlos A. Bacino
Guney Bademci
Eva Baker
Ashok Balasubramanyam
Dustin Baldridge
Jim Bale
Michael Bamshad
Deborah Barbouth
Pinar Bayrak-Toydemir
Anita Beck
Alan H. Beggs
Edward Behrens
Gill Bejerano
Jimmy Bennet
Beverly Berg-Rood
Jonathan A. Bernstein
Gerard T. Berry
Anna Bican
Stephanie Bivona
Elizabeth Blue
John Bohnsack
Carsten Bonnenmann
Devon Bonner
Lorenzo Botto
Brenna Boyd
Lauren C. Briere
Elly Brokamp
Gabrielle Brown
Elizabeth A. Burke
Lindsay C. Burrage
Manish J. Butte
Peter Byers
William E. Byrd
John Carey
Olveen Carrasquillo
Ta Chen Peter Chang
Sirisak Chanprasert
Hsiao-Tuan Chao
Gary D. Clark
Terra R. Coakley
Laurel A. Cobban
Joy D. Cogan
Matthew Coggins
F. Sessions Cole
Heather A. Colley
Cynthia M. Cooper
Heidi Cope
William J. Craigen
Andrew B. Crouse
Michael Cunningham
Precilla D'Souza
Hongzheng Dai
Surendra Dasari
Joie Davis
Jyoti G. Dayal
Matthew Deardorff
Esteban C. Dell'Angelica
Katrina Dipple
Daniel Doherty
Naghmeh Dorrani
Argenia L. Doss
Emilie D. Douine
David D. Draper
Laura Duncan
Dawn Earl
David J. Eckstein
Lisa T. Emrick
Christine M. Eng
Cecilia Esteves
Marni Falk
Liliana Fernandez
Carlos Ferreira
Elizabeth L. Fieg
Laurie C. Findley
Paul G. Fisher
Brent L. Fogel
Irman Forghani
William A. Gahl
Ian Glass
Bernadette Gochuico
Rena A. Godfrey
Katie Golden-Grant
Madison P. Goldrich
David B. Goldstein
Alana Grajewski
Catherine A. Groden
Irma Gutierrez
Sihoun Hahn
Rizwan Hamid
Kelly Hassey
Nichole Hayes
Frances High
Anne Hing
Fuki M. Hisama
Ingrid A. Holm
Jason Hom
Martha Horike-Pyne
Alden Huang
Yong Huang
Laryssa Huryn
Rosario Isasi
Fariha Jamal
Gail P. Jarvik
Jeffrey Jarvik
Suman Jayadev
Lefkothea Karaviti
Jennifer Kennedy
Shamika Ketkar
Dana Kiley
Shilpa N. Kobren
Isaac S. Kohane
Jennefer N. Kohler
Deborah Krakow
Donna M. Krasnewich
Elijah Kravets
Susan Korrick
Mary Koziura
Joel B. Krier
Seema R. Lalani
Byron Lam
Christina Lam
Grace L. LaMoure
Brendan C. Lanpher
Ian R. Lanza
Lea Latham
Kimberly LeBlanc
Brendan H. Lee
Hane Lee
Roy Levitt
Richard A. Lewis
Sharyn A. Lincoln
Pengfei Liu
Xue Zhong Liu
Nicola Longo
Sandra K. Loo
Joseph Loscalzo
Richard L. Maas
John MacDowall
Ellen F. Macnamara
Calum A. MacRae
Valerie V. Maduro
Bryan C. Mak
May Christine V. Malicdan
Laura A. Mamounas
Teri A. Manolio
Rong Mao
Kenneth Maravilla
Thomas C. Markello
Ronit Marom
Gabor Marth
Beth A. Martin
Martin G. Martin
Julian A. Martínez-Agosto
Shruti Marwaha
Jacob McCauley
Allyn McConkie-Rosell
Alexa T. McCray
Elisabeth McGee
Heather Mefford
J. Lawrence Merritt
Matthew Might
Ghayda Mirzaa
Eva Morava
Paolo M. Moretti
Deborah Mosbrook-Davis
John J. Mulvihill
Mariko Nakano-Okuno
Avi Nath
Stan F. Nelson
John H. Newman
Sarah K. Nicholas
Deborah Nickerson
Shirley Nieves-Rodriguez
Donna Novacic
Devin Oglesbee
James P. Orengo
Laura Pace
Stephen Pak
J. Carl Pallais
Christina GS. Palmer
Jeanette C. Papp
Neil H. Parker
John A. Phillips III
Jennifer E. Posey
Lorraine Potocki
Bradley Power
Barbara N. Pusey
Aaron Quinlan
Wendy Raskind
Archana N. Raja
Deepak A. Rao
Genecee Renteria
Chloe M. Reuter
Lynette Rives
Amy K. Robertson
Lance H. Rodan
Jill A. Rosenfeld
Natalie Rosenwasser

Francis Rossignol
Maura Ruzhnikov
Ralph Sacco
Jacinda B. Sampson
Mario Saporta
C. Ron Scott
Judy Schaechter
Timothy Schedl
Kelly Schoch
Daryl A. Scott
Vandana Shashi
Jimann Shin
Rebecca Signer
Edwin K. Silverman
Janet S. Sinsheimer
Kathy Sisco
Edward C. Smith
Kevin S. Smith
Emily Solem
Lilianna Solnica-Krezel
Ben Solomon
Rebecca C. Spillmann
Joan M. Stoler
Jennifer A. Sullivan
Kathleen Sullivan
Angela Sun
Shirley Sutton
David A. Sweetser
Virginia Sybert
Holly K. Tabor
Amelia L. M. Tan
Queenie K.-G. Tan
Mustafa Tekin
Fred Telischi
Willa Thorson
Audrey Thurm
Cynthia J. Tifft
Camilo Toro
Alyssa A. Tran
Brianna M. Tucker
Tiina K. Urv
Adeline Vanderver
Matt Velinder
Dave Viskochil
Tiphanie P. Vogel
Colleen E. Wahl
Stephanie Wallace
Nicole M. Walley
Chris A. Walsh
Melissa Walker
Jennifer Wambach
Jijun Wan
Lee-kai Wang
Michael F. Wangler
Patricia A. Ward
Daniel Wegner
Monika Weisz-Hubshman
Mark Wener
Tara Wenger
Katherine Wesseling Perry
Monte Westerfield
Matthew T. Wheeler
Jordan Whitlock
Lynne A. Wolfe
Jeremy D. Woods
Kim Worley
Shinya Yamamoto
John Yang
Muhammad Yousef
Diane B. Zastrow
Wadih Zein
Chunli Zhao
Stephan Zuchner
Hugo Bellen
Rachel Mahoney

REFERENCES

1. Bacher, U., Haferlach, T., Schoch, C., Kern, W. & Schnittger, S. Implications of NRAS mutations in AML: a study of 2502 patients. *Blood* **107**, 3847-53 (2006).
2. Janssen, J.W. *et al.* RAS gene mutations in acute and chronic myelocytic leukemias, chronic myeloproliferative disorders, and myelodysplastic syndromes. *Proc Natl Acad Sci U S A* **84**, 9228-32 (1987).
3. Li, Q. *et al.* Interpretation of 'Omics dynamics in a single subject using local estimates of dispersion between two transcriptomes. *AMIA Annu Symp Proc* **2019**, 582-591 (2019).
4. Regan, J.F. *et al.* A rapid molecular approach for chromosomal phasing. *PLoS One* **10**, e0118270 (2015).
5. Ferreira, M.S.V. *et al.* Comparison of flow-FISH and MM-qPCR telomere length assessment techniques for the screening of telomeropathies. *Ann N Y Acad Sci* **1466**, 93-103 (2020).
6. de Pauw, E.S. *et al.* Assessment of telomere length in hematopoietic interphase cells using in situ hybridization and digital fluorescence microscopy. *Cytometry* **32**, 163-9 (1998).
7. Lai, T.P. *et al.* A method for measuring the distribution of the shortest telomeres in cells and tissues. *Nat Commun* **8**, 1356 (2017).
8. Henricksen, L.A., Umbricht, C.B. & Wold, M.S. Recombinant replication protein A: expression, complex formation, and functional characterization. *J Biol Chem* **269**, 11121-32 (1994).
9. Grimme, J.M. & Spies, M. FRET-based assays to monitor DNA binding and annealing by Rad52 recombination mediator protein. *Methods Mol Biol* **745**, 463-83 (2011).
10. Ying, L., Green, J.J., Li, H., Klenerman, D. & Balasubramanian, S. Studies on the structure and dynamics of the human telomeric G quadruplex by single-molecule fluorescence resonance energy transfer. *Proc Natl Acad Sci U S A* **100**, 14629-34 (2003).
11. Beers, J. *et al.* A cost-effective and efficient reprogramming platform for large-scale production of integration-free human induced pluripotent stem cells in chemically defined culture. *Sci Rep* **5**, 11319 (2015).
12. Chen, G. *et al.* Chemically defined conditions for human iPSC derivation and culture. *Nat Methods* **8**, 424-9 (2011).
13. Paluru, P. *et al.* The negative impact of Wnt signaling on megakaryocyte and primitive erythroid progenitors derived from human embryonic stem cells. *Stem Cell Res* **12**, 441-51 (2014).
14. Connelly, J.P. & Pruett-Miller, S.M. CRIS.py: A Versatile and High-throughput Analysis Program for CRISPR-based Genome Editing. *Sci Rep* **9**, 4194 (2019).
15. Ruiz, J.P. *et al.* Robust generation of erythroid and multilineage hematopoietic progenitors from human iPSCs using a scalable monolayer culture system. *Stem Cell Res* **41**, 101600 (2019).